A Novel Method of Using Iron Nanoparticles from Coal Fly Ash or Ferric Chloride for Acid Mine Drainage Remediation

Crisanda Gilbert[1] · Olushola S. Ayanda[2,3] · Olanrewaju O. Fatoba[1] · Godfrey Madzivire[4] · Leslie F. Petrik[1]

Abstract

Iron nanoparticles (nano Fe) were extracted from coal fly ash (CFA) or ferric chloride ($FeCl_3$) and used for acid mine drainage (AMD) remediation. Characterisation was achieved by X-ray diffraction (XRD), X-ray fluorescence, scanning electron microscopy-energy dispersive spectroscopy (SEM–EDX), high resolution transmission electron microscopy (HRTEM), and the Braunaer–Emmet–Teller (BET) surface area determination. The HRTEM indicated good dispersion of the characteristic bead-like structure of nano Fe. It was also observed that the nano Fe were mainly in the zero-valent oxidation state, as denoted by the characteristic peak at $\approx 44.7°$ in the XRD analysis; it was accompanied by the generally accepted oxide layer around the particles, which was confirmed by the appearance of a core–shell structure in the HRTEM micrographs. The BET surface areas of the nano Fe extracted from the CFA or $FeCl_3$ were recorded to be 34.7 or 88.8 m^2/g, respectively. The nano Fe lowered the concentration of most of the monitored contaminants, with the percentage removal ranging from 17 to 99%. The pH of the AMD after treatment with nano Fe obtained from CFA or $FeCl_3$ increased to 5.74 or 6.01, respectively, from 3.49, the electrical conductivity decreased to 0.18 or 0.13 Ω/m, respectively from 0.57 Ω/m, while the total dissolved solids was decreased to 447 or 384 mg/L, respectively, from 1683 mg/L. The water quality of the treated AMD is suitable for Category 4 industrial use, per the Dept. of Water Affairs and Forestry's limits.

Keywords Extraction · Characterisation · Nano-iron · Coal mining · Coal power station

Introduction

Coal-fired power stations account for 93% of South Africa's energy production, with Eskom being the major power utility (Eberhard 2011). The burned coal leaves an incombustible

✉ Olushola S. Ayanda
  osayanda@gmail.com

1   Environmental and Nano Science Research Group, Department of Chemistry, University of the Western Cape, Private Bag X17, Bellville, South Africa

2   Department of Chemistry, Vaal University of Technology, Vanderbijlpark 1900, South Africa

3   Nanoscience Research, Department of Industrial Chemistry, Federal University Oye Ekiti, P.M.B 373, Oye Ekiti, Ekiti, Nigeria

4   Environmental Geosciences, Council for Geoscience, Pretoria, South Africa

inorganic waste known as coal fly ash (CFA), which is a by-product of the coal combustion process. CFA can contain toxic metals as well as rare earth elements (Sahoo et al. 2016) due to the inorganic fraction (detrital and authigenic minerals) of the parent coal (Groen and Craig 1994). Because of its hazardous nature, CFA is currently being deposited on ash dumps and is often co-disposed with brines originating from the water treatment circuits at power stations in South Africa. However, the leaching of the toxic elements and salts from CFA into the soil and water tables can subsequently affect the eco-systems surrounding the contaminated area (Kapoor and Christian 2016). It is particularly difficult to dispose of CFA in an environmentally sustainable way due to the composition of the ash. Therefore, new methods for its beneficiation and utilisation are being explored through research.

Coal mining also can generate acid mine drainage (AMD). AMD is a complex pollutant characterised by high concentrations of iron and sulphate, a low pH, and elevated concentrations of a wide variety of metals, depending on the host rock geology (Gray 1998). AMD occurs due to

the oxidation and hydrolysis of pyrite in underground mine shafts (Fashola et al. 2016), open pits, mine dumps, tailings, and ore stockpiles. Currently, the South African mining sector has to comply with strict legislation, such as SANS 10234 (DWAF 2005), with respect to its waste material. This involves cleaning all wastewater to a high quality before it can be released into the environment.

CFA can be classified as either Class F or Class C. Class F CFA is produced by burning bituminous and anthracite coal and contains less than 7% lime (CaO), while the total amount of SiO_2, Al_2O_3, and Fe_2O_3 is greater than or equal to 70 wt. %. Class C CFA is generally produced from burning lignite or sub-bituminous coal, contains more than 20% lime, and between 50 to 70 wt. % of SiO_2, Al_2O_3, and Fe_2O_3 (Pradoto et al. 2016). South Africa's CFA is classified as class F (Gitari et al. 2006).

There have been many attempts to selectively recover elements of value from CFA, including: germanium (Torralvo and Fernández-Pereira 2011), gallium and vanadium (Font et al. 2007), aluminium (Wu et al. 2006), and boron (Polowczyk et al. 2013). We considered the production of iron nanoparticles (nano Fe) as worth investigating since iron (Fe) is one of the major components of the CFA and has been isolated from CFA by dry magnetic separation (Dai et al. 2015). Contemporary studies (e.g. Mattigod et al. 1990; Shoumkova 2011) have also suggested the recovery of hematite and magnetite from fly ash.

Producing nano Fe from CFA was considered since the preparation of nano Fe from ferric salts on a large scale is expensive (Cao et al. 2012). Common techniques to produce nano Fe include: mercury-based methods (Ali et al. 2016), thermal decomposition (Hufschmid et al. 2015), sonochemical decomposition (Dolores et al. 2015), reduction of iron salts and oxides (Huber 2005), inverse micelle (Carpenter 2001), vapour phase deposition (Brooke et al. 2017), and mechanical methods (Kerekes et al. 2002). The extraction of nano Fe from an iron-rich waste material would promote its beneficiation (Farhanian et al. 2014), and is attractive because nano Fe can be used for wastewater treatment, in permeable reactive barriers (Mueller and Nowack, 2010), and to destroy or stabilise halogenated hydrocarbons (Zhang 2003), carbon tetrachloride (Nurmi et al. 2005), and polychlorinatedbiphenyls (Varanasi et al. 2007), and a wide array of common environmental contaminants like chlorinated organic solvents (Nutt et al. 2005), organochlorine pesticides (Elliott et al. 2003), organic dyes (Liu et al. 2005), various inorganic compounds (Cao et al. 2005), and metal ions (Li and Zhang 2007; Ponder et al. 2000). Nano Fe can also be used as catalyst and as primary colorant in glass and ceramics, and is used in certain alloys, memory tape, coatings, and medical and laboratory applications. The reductive properties of elemental iron can also be used to reduce metal concentrations in water through changes in their oxidation state and/or by adsorption (Geng et al. 2009; Shih and Tai 2010).

Therefore, the aim of this study was to extract nano Fe from CFA and to compare it with nano Fe produced from a commercial reagent for treatment of AMD. Using CFA as a feedstock for the production of nanomaterials is an attractive concept, while AMD treatment by nano Fe also supports the need to develop innovative ways to use CFA. Moreover, this research enables the use of a waste to remediate a waste.

Materials and Methods

Coal Fly Ash and Acid Mine Drainage

The CFA sample was collected from the Hendrina coal fired power stations, Mpumalanga Province, South Africa. The AMD was collected from Shaft 8, Rand Uranium Gold mine, Gauteng, South Africa and was filtered through 0.45 μm pore Whatmann's filter paper. The locations of the Hendrina coal-fired power stations and Rand Uranium Gold mine are presented Fig. 1a, b, respectively. Ferric chloride ($FeCl_3 \cdot 6H_2O$), hydrochloric acid (HCl), sodium borohydride ($NaBH_4$) and the filter paper were supplied by Kimix Chemical & Lab Supplies, South Africa.

Extraction of Iron Oxide from Coal Fly Ash

The extraction of Fe from CFA involved measuring 100 g of CFA into a plastic beaker, to which 200 mL of deionised water (conductivity = 0.055 μS/cm) was added. The slurry was initially mixed with a stirring rod, after which a magnetic stirring bar was used at a constant speed of 250 rpm for 30 min. After this, the magnetic stirrer was removed and a bar magnet was used to attract the Fe oxide that had been liberated from the CFA. The solid residue, which was essentially the non-magnetic fraction of the CFA, was collected by vacuum filtration using a Buschner funnel, while the filtrate (supernatant liquid) was collected in the flask. The Fe oxide fraction was washed several times with deionised water, after which it was dried in an oven at 70 °C for 24 h. Stirring times of 30, 60, 120, 180, 360, 720, and 1440 min were investigated and the yield in each case was evaluated to ascertain the optimal stirring time.

Digestion and Precipitation of Iron Nanoparticles

The Fe oxide obtained from the CFA was in a granular form and still included impurities, such as silica and aluminium. Therefore, 5.0 g of the magnetically extracted iron was dissolved using the total acid (conc. HCl) digestion technique. The resulting digestate was filtered through a 0.45 μm
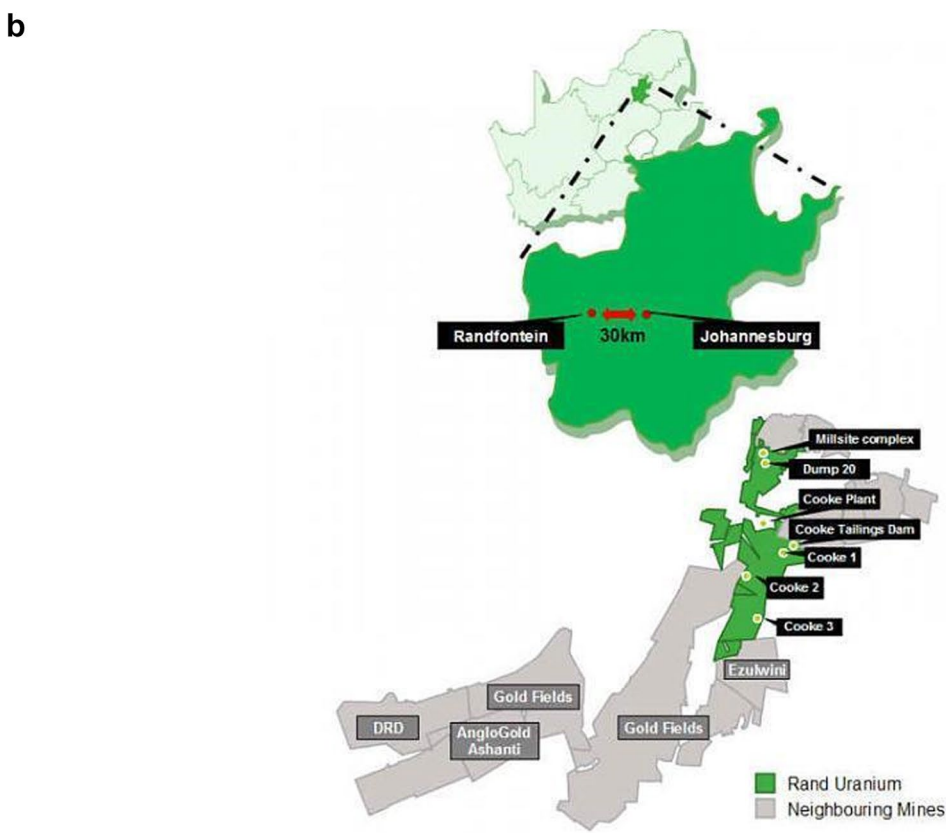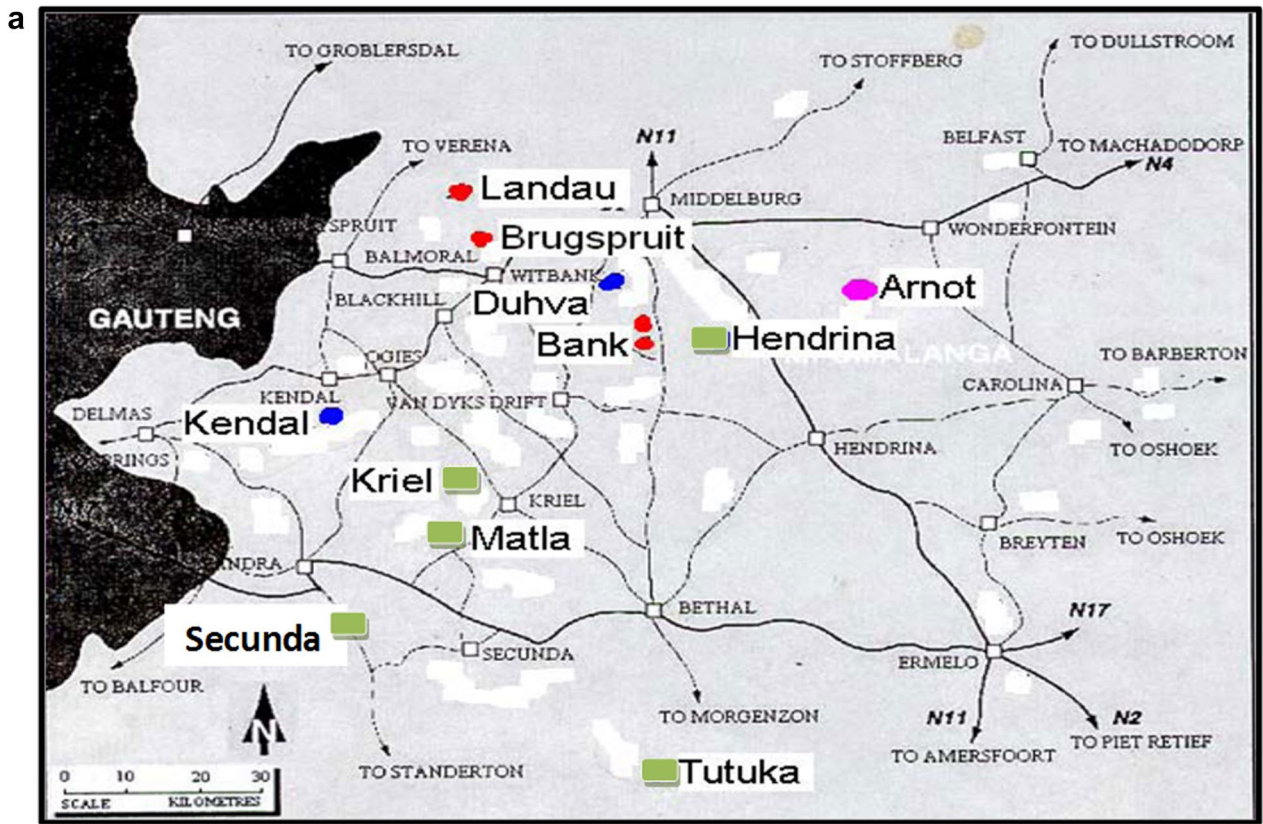
Fig. 1 Location of the study area where CFA (**a**) and AMD (**b**) were collected

membrane filter paper and the filtrate was decanted into a 1 L volumetric flask and made up to the mark with deionised water. The digested CFA iron solution was used as a feedstock for the reduction process.

The reduction process involved transferring 50 mL of the digested Fe solution into a 200 mL beaker to which 0.01 M $NaBH_4$ was titrated drop-wise to induce precipitation of nano Fe. The magnetic stirrer was set at a constant speed of 250 rpm. The addition of the $NaBH_4$ caused the solution to turn black, which signaled precipitation, and was accompanied by bubbles, which were presumed to be due to the liberation of hydrogen (Eq. 1).

$$4\,Fe^{3+} + 3\,BH_4^- + 9\,H_2O\ \rightarrow\ 4\,Fe^0 + 3\,H_2BO_3^- + 12\,H^+ + 6\,H_2 \tag{1}$$
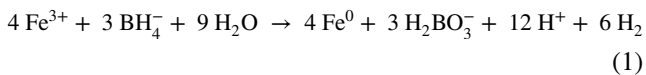
The reaction was judged to be complete once the bubble formation stopped. The nano Fe was collected using a bar magnet and washed with deionised water. The resulting solid was dried under nitrogen. The optimum concentration of $NaBH_4$ was investigated using different concentrations of $NaBH_4$ solutions (0.01–0.1 M), while the volume was fixed at 100 mL.

Production of Iron Nanoparticles from Chemical Reagents

24 g of ferric chloride ($FeCl_3$) was weighed into a 500 mL beaker and dissolved in 200 mL deionised water to make up a 0.1 M solution. After complete dissolution, the solution was transferred into a 1 L volumetric flask and made up to the mark with deionised water. 50 mL of the solution was transferred into a 200 mL beaker to which 100 mL of 0.01 M $NaBH_4$ was added drop-wise to induce precipitation of nano Fe. The magnetic stirrer was set at a constant speed of 250 rpm. Again, the addition of $NaBH_4$ caused the solution to darken, indicating precipitation, and was accompanied by the bubble formation. The optimum concentration of $NaBH_4$ was also investigated at different concentrations of $NaBH_4$ solutions (0.01–0.1 M).

Once the effervescence ceased, the stirrer was removed and a bar magnet was used to localise the Fe that had precipitated. The resulting liquor was decanted and the iron was washed with deionised water. Finally, the Fe was dried under nitrogen to avoid rapid oxidation.

Instrumentation

The CFA, Fe oxide extracted from CFA, and the two versions of the nano Fe were analysed by the use of X-ray diffraction (XRD; Siemens D8 Advance Bruker AXSI instrument) and X-ray fluorescence (XRF; Philips 1404 Wavelength Dispersive Spectrometer fitted with an Rh tube) for mineralogy and elemental composition, respectively. The morphologies were examined using scanning electron microscopy (SEM; Nova Nano SEM 230) equipped with an Oxford X-max detector and software for elemental analysis by energy dispersive spectroscopy (EDS). The SEM was accompanied by a high resolution transmission electron microscope (HRTEM; TECNAI G2 F20 X Twin Mat FEG), while the surface area was examined using N_2 Brunauer–Emmet–Teller (BET) adsorption. The AMD and the filtrates generated after the treatment processes were analysed using ion chromatography (IC; Dionex ICS-1600 ion chromatograph with ion pack AS 14A column and AG 14–4 mm guard column) for anions, and inductively-coupled plasma-optical emission spectroscopy (ICP-OES; Variance Liberty II) for cations and other elements. The pH, electrical conductivity (EC), and total dissolved solids (TDS) of the AMD were also carried using a Hanna HI 9828 pH meter with a portable pH/EC/TDS/DO/temperature probe.

Treatment of the Acid Mine Drainage

The nano Fe obtained from CFA or commercial reagents were both tested for their use in treating AMD to compare their efficacy. The extracted nano Fe were dried in an oven at 50 °C for 12 h to remove all traces of moisture, and then weighed and transferred into separate 100 mL Erlenmeyer flasks. Each of the samples was prepared in triplicate and 50 mL of raw AMD was added to each flask. A blank sample was also prepared by adding 50 mL of AMD into an empty flask without any nano Fe. The flasks were placed in an agitator operated at 250 rpm at room temperature (2 5 °C) for 24 h. The nano Fe were removed from the agitator after the reaction contact time had been completed. The mixture was filtered using 0.45 µm membrane filter paper and the filtrate analyzed using ICP-OES and IC. The percentage removal was calculated by Eq. (2).

$$\%Removal = \frac{C_o - C_f}{C_o} \times 100 \tag{2}$$

where Co and C_f are the initial and final concentrations of a contaminant, respectively. The nano Fe dosage (0.05, 0.1, 0.3, and 0.5 g) and treatment contact time (10, 30, 60, 120, 240, and 1440 min) were optimised to refine the process.

Results and Discussion

Characterisation of Coal Fly Ash

SEM was used to analyse the surface morphology of the CFA, while HRTEM revealed the internal morphology of the sample. The SEM micrograph of the raw CFA (see supplemental Figure S-1) show that the CFA consisted mainly

of spherical particles (cenospheres) with diameters ranging from 0.25 to 10 µm. Accompanying the spherical particles were irregularly shaped particles, which are typical of CFA samples, as the defects in the spheres are thought to be due to inter-particle contact during rapid cooling (Wang et al. 2008).

Elemental analysis by EDS suggested that the most prevalent elements in the raw CFA were Si, Al, Ca, Fe, O, S, K, Ti, and Na (supplemental Figure S-2). The Al and Si peaks were dominant, but EDS analysis is not an accurate representation of quantitative composition. For this reason, XRF was used to determine the CFA's elemental composition.

The HRTEM micrograph of the CFA structure (supplemental Figure S-3) shows spherical particles along with some irregular shaped masses, which appear to be due to agglomeration of smaller spheres. The SAED spectrum indicated faint concentric rings with random bright spots. This suggests that Hendrina CFA is polycrystalline in nature (Silva et al. 2009; Üzüm et al. 2009).

The XRF analysis of the CFA identified SiO_2 and Al_2O_3 as the major oxides present in the CFA, followed by oxides of calcium and iron (Table 1). This was corroborated qualitatively by the XRD, which identified the major crystal phases as mullite ($3Al_2O_3 \cdot 2SiO_2$) and quartz (SiO_2), which corresponded to the abundance of Al and Si. However, the iron-bearing mineral (hematite, Fe_2O_3) is the species of interest in this study.

Analysis of the Acid Mine Drainage

The physical characteristics and the composition of the AMD, as determined by ICP-OES and IC, are presented in Tables 2 and 3, respectively. The pH (3.49), EC (5.74 Ω/m),

Table 1 Elemental composition of major species present in Hendrina coal fly ash

Species	Hendrina CFA (% w/w composition)
SiO_2	54 ± 1
Al_2O_3	26.1 ± 0.1
CaO	4.80 ± 0.03
SO_3	4.78 ± 0.04
Fe_2O_3	4.5 ± 0.1
MgO	1.8 ± 0.1
TiO_2	1.3 ± 0.1
K_2O	0.79 ± 0.02
P_2O_5	0.56 ± 0.03
MnO	0.04 ± 0.00
Na_2O	0.03 ± 0.01
Cr_2O_3	0.03 ± 0.01
Loss on ignition (LOI)	1.2 ± 0.1
Total	99.93

Table 2 Physical attributes of AMD

Parameter	Units	Rand Uranium mine water
pH		3.49 ± 0.01
EC	Ω/m	5.7 ± 0.1
TDS	mg/L	1683 ± 0.0

and TDS are also listed. The AMD is rich in Fe, Na, Ca, and K, and also contains considerable amounts of Mn and Mg. Chloride and nitrate exceeded the accepted limits of 5 and 10 mg/L, respectively, for potable water (WHO 2011).

Extraction of Iron

After completion of the Fe separation, the CFA slurry was present as three fractions: the magnetic portion, the non-magnetic solid residue, and the filtrate. The Fe content in the CFA was ≈ 4.52% (Table 1). Therefore, theoretically, 100 g of CFA should yield approximately 4.52 g of Fe oxide.

The yield and percentage recovery of Fe obtained from 100 g of CFA revealed an increased yield as stirring time was increased (Fig. 2). Experimental data indicated that a stirring time of 6 h yielded 3.74 g of the magnetic Fe oxide fraction and a recovery of 82%, whereas stirring for 24 h resulted in 4.03 g and a recovery of 89%. Since all of the Fe oxide could still not be recovered in 24 h, and yield was not substantially higher, the extended time frame and energy consumption was not justified. Thus, a stirring time of 6 h was adopted for continuation of the extraction process. Once extraction was completed, the various fractions produced by magnetic separation were characterised.

The SEM image of the magnetically extracted granular Fe (supplemental Figure S-4a and b) depicts globular structures ≈ 1 µm or less in diameter. The Fe extracted at this stage was not pure, since the Fe spheres/globules consisted of Fe oxide mixed with amorphous aluminosilicate material. The SEM micrograph of the non-magnetic fly ash solid residue (supplemental Figure S-4c) shows spherical particles, which are characteristic of CFA, and contained mostly Al and Si, according to ICP-OES analysis of the CFA solid residue. Supplemental Figure S-4d depicted layered surfaces with jagged edges present in the solid residue after extraction, quite different from the morphology of the granular iron. This material is thought to be thermally decomposed mullite ($3Al_2O_3 \cdot 2SiO_2$), produced during the high temperatures involved in CFA (Xiao and Mitchell 2000).

The elemental composition of the magnetically extracted granular Fe and the non-magnetic solid residue as assessed by XRF is presented in Table 4. Analysis of the elemental composition highlighted the changes that occurred in the CFA residue after the magnetic extraction.

Table 3 Elemental composition of AMD

Elements	AMD (mg/L)
Ca	1141 ± 13
Na	345 ± 5
Mg	299 ± 7
K	271 ± 5
Fe	221 ± 7
Mn	104 ± 5
Si	74 ± 6
B	25 ± 2
Hg	18 ± 2
Li	6.9 ± 0.2
Al	5.2 ± 0.1
Se	3.9 ± 0.5
U	2.9 ± 0.1
Th	2.2 ± 0.3
Zn	1.4 ± 0.8
Ni	1.9 ± 0.3
Co	1.3 ± 0.1
Ce	1.1 ± 0.1
P	0.9 ± 0.3
Sr	0.8 ± 0.1
Pb	0.8 ± 0.3
Ba	0.8 ± 0.1
As	0.8 ± 0.2
Cr	0.8 ± 0.1
Cu	0.65 ± 0.04
Mo	0.24 ± 0.02
Rb	0.20 ± 0.01
Ti	0.19 ± 0.02
Nb	0.17 ± 0.04
Y	0.10 ± 0.06
Zr	0.12 ± 0.03
V	0.06 ± 0.02
Cd	0.04 ± 0.01
Be	0.03 ± 0.01
Anions	Concentration (mg/L)
Cl^-	90.9 ± 0.2
NO^{3-}	56 ± 1
SO_4^{2-}	4959 ± 115
PO_4^{3-}	ND

ND not detected

The XRF analysis of the magnetically extracted Fe concentrate revealed that the extract was composed primarily of Fe, but still contained small amounts of Al and Si. Some iron-bearing phases may have been trapped within aluminosilicates due to the high temperatures involved in CFA generation, causing these impurities to be transferred into the magnetic fraction along with the iron. Kutchko and

Kim (2006) suggested that the Fe oxide in some instances is not a surface phenomenon on the aluminosilicate material, but is rather an integral part of the solid particle. Analysis of the solid CFA residue remaining after magnetic extraction revealed that Al and Si were the predominant species, much like the raw CFA; however, Fe concentrations significantly decreased due to the partitioning effect of the magnetic portion during the extraction.

The filtrate recovered after extraction of the Fe fraction was analyzed by ICP-OES (supplemental Table T-1). This aqueous portion contained traces of the various soluble elements present in the CFA. The concentration of particular elements in the supernatant was thought to have been influenced by their solubility in the solvent (deionised water). Calcium dominated the composition of the supernatant, since it rapidly dissolves in contact with aqueous media (Choi et al. 2002). The mineral phases present in the granular Fe extract were determined using XRD and confirmed the recovery of the Fe-bearing phases by magnetic separation (Fig. 3).

The XRD pattern of the magnetic portion extracted from the CFA revealed an iron-rich material primarily composed of hematite (Fe_2O_3) and maghemite (γ-Fe_2O_3). Since the magnetic separation does not involve the use of any chemicals, it can be assumed that no chemical transformations occurred. The additional Si and Al mineral phases present were the quartz (SiO_2) and mullite ($3Al_2O_3 \cdot 2SiO_2$), which were not removed by magnetic separation.

The BET results (Table 5) revealed that the extracted Fe oxide concentrate samples were macroporous and had a low total surface area of 1.34 m²/g, which was less than some values reported in the literature (Gui et al. 2000; Jeen et al. 2006; Scherer et al. 2001). Most of the surface area (1.32 m²/g) was external, and the pore volume of the recovered iron oxide concentrates was found to be very low, at 0.00001 m³/g.

Iron Precipitation

Following extraction and separation of Fe oxide from the raw CFA, total acid digestion of the iron concentrate was necessary prior to producing nano Fe below the 100 nm range. The granular Fe extracted by magnetic separation after 6 h of stirring was used as the precursor for nano Fe generation. The purpose of this experiment was to optimise the conditions required to obtain a viable nanoparticle yield from the digested iron extract whilst using the least amount of reductant. The use of excessive amounts of chemicals was avoided by optimising the process. For the granular iron digestate, Fig. 4 indicates that the yield of nano Fe increased steadily with $NaBH_4$ concentration up to 0.06 M, after which the graph began to flatten, indicating that the increased concentration of $NaBH_4$ was not returning a higher yield of nano

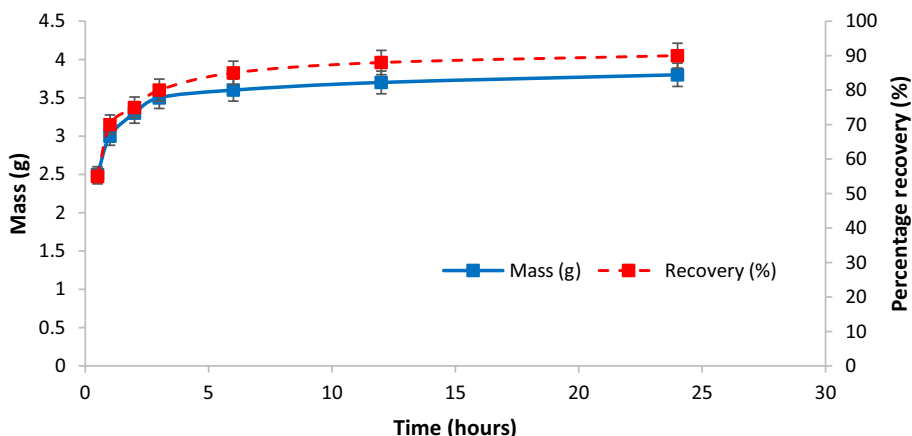**Fig. 2** Yield and percentage recovery of iron from 100 g of CFA

Table 4 Elemental composition of major species present as oxides in the various solid fractions produced from the magnetic separation of Hendrina coal fly ash

Species	Hendrina iron concentrate (% w/w composition)	Solid residue after extraction (% w/w composition)
Fe_2O_3	93 ± 2	1.6 ± 0.1
SiO_2	2.3 ± 0.1	58 ± 1
Al_2O_3	2.1 ± 0.1	26.8 ± 0.1
MgO	0.18 ± 0.07	2.80 ± 0.03
P_2O_5	0.11 ± 0.06	0.4 ± 0.1
Na_2O	0.10 ± 0.04	0.05 ± 0.01
Cr_2O_3	0.09 ± 0.03	1.12 ± 0.02
TiO_2	0.09 ± 0.02	0.56 ± 0.03
CaO	0.08 ± 0.02	6.2 ± 0.2
MnO	0.05 ± 0.02	0.03 ± 0.01
SO_3	0.05 ± 0.01	0.04 ± 0.01
K_2O	0.04 ± 0.01	1.0 ± 0.1
LOI	0.9 ± 0.1	1.1 ± 0.1
Total	99.09	99.70

Fe, and thus all available Fe was precipitated from solution. For this reason, the 0.06 M solution of $NaBH_4$, which yielded 0.31 g of nano Fe per 50 mL of 0.12 M granular Fe solution, was considered to be the optimal concentration for the remainder of this series of experiments. The use of higher concentrations of reductant was not necessary as the yield of nano Fe was only marginally better than that of the 0.06 M $NaBH_4$.

The nano Fe generated from the granular Fe digestate was compared to that from 50 mL of the 0.1 M $FeCl_3$ to determine if the quality of the nano Fe produced from a waste material could rival that made from chemical grade reagents.

The amount of reductant required to induce precipitation of nano iron from $FeCl_3$ (Fig. 4) showed a steady increase in yield with increasing concentration up to 0.08 M, after which the increase was minimal. Approximately 0.33 g of nano Fe was produced from 50 mL of 0.1 M $FeCl_3$ solution at the 0.08 M concentration, whereas a 1.0 M solution merely yielded an additional 0.01 g. This suggested that a

Fig. 3 X-ray diffraction analysis of CFA, CFA residue and magnetically extracted granular iron
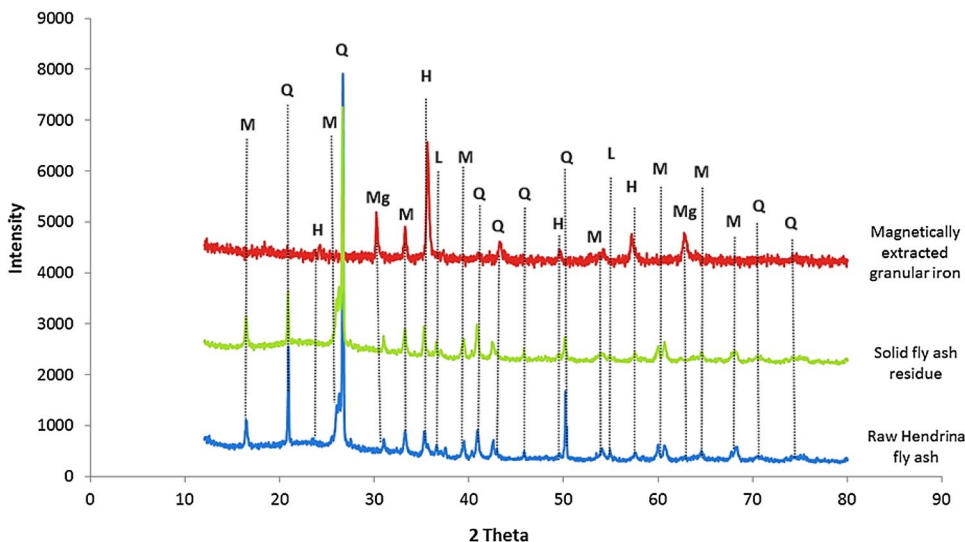
0.08 M solution of $NaBH_4$ would suffice and thus this concentration was used for the rest of the experiment.

Reduction of both the granular Fe digestate as well as the $FeCl_3$ solution by $NaBH_4$ resulted in a similar yield of nano Fe. This suggests that the granular iron digestate was of similar quality to the $FeCl_3$ chemical reagent solution. Thus, the two forms of nano Fe were characterised to understand their physical and chemical properties.
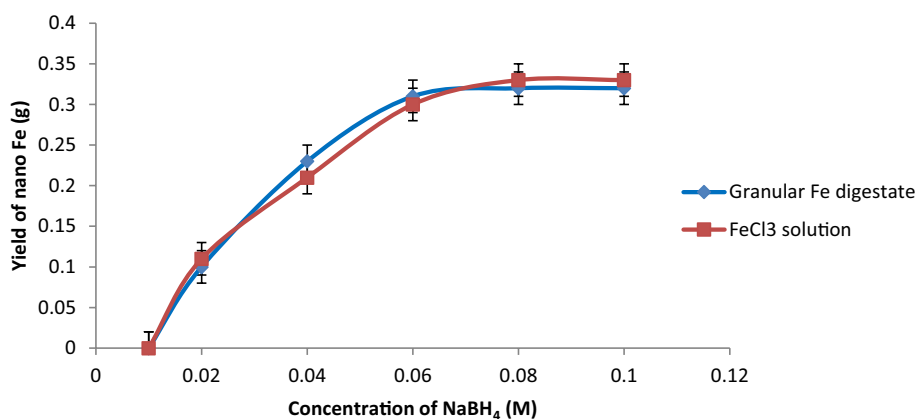
The SEM micrographs of the nano Fe generated from both sources (Fig. 5) revealed agglomerations of densely packed semi-spherical particles, which is in accordance the work of others (Huang and Ehrman 2007; Shahwan et al. 2010). Aggregation of nanoparticles was reported to be caused by the large surface area and magnetic dipole–dipole interactions of the individual particles (Li et al. 2006). The structures appeared to consist of semi-spherical particles on the nanoscale. This was confirmed by HRTEM (Fig. 6).

The HRTEM micrographs (Fig. 6a and c) of the nano Fe from CFA or $FeCl_3$ look similar, being comprised of aggregates of plates (Fig. 7) and smaller irregular particles with diameters ranging from 30 to 50 nm, some of which formed characteristic chain-like structures. The plates, which appear to be oxides, looked larger than the particles and varied in size and quantity. These findings concur with Nurmi et al. (2005) and Üzüm et al. (2009). The selected area electron diffraction (SAED) patterns for both sources of nano Fe (Fig. 6b, d) suggested that the absence of lattice fringes and the diffuse rings are an indication that they are polycrystalline (Wang et al. 2009).

Li et al. (2006) indicated that nano Fe possesses a core–shell structure, in which the shell is an oxidised layer that surrounds the Fe^0 core and protects it from further oxidation. The HRTEM analysis supported this and indicated that the shell was about 5 nm thick, in line with previously reported values (Kim et al. 2010; Martin et al. 2008).

The qualitative elemental composition of nano Fe precipitated from CFA or $FeCl_3$ by the EDS (Fig. 8a, b) suggested that both samples were composed primarily of Fe, with the Fe obtained from granular Fe digestate (FANI) containing traces of Al, which could have been carried over from the granular CFA Fe precursor since the magnetic separation was a physical separation, which lacks the selectivity of a chemical separation. The only notable difference in the Fe obtained from $FeCl_3$ (FCLI) is the inclusion of a chloride peak, which is absent in the Fe extracted from granular digestate. This peak was most likely due to the $FeCl_3$ precursor from which the nanoparticles had precipitated. The presence of oxygen in both spectrums may allude to the nature of the nano Fe core–shell, with the presence of carbon (C) due to carbonisation of the sample before SEM–EDS analysis.

Quantitative analyses using ICP-OES and IC (Fig. 8c, d) confirmed the dominance of Fe (77.31 wt%), with a significant Al content (5.75 wt%) for the nano Fe precipitated from the magnetically extracted granular Fe from CFA. The nano Fe precipitated from the $FeCl_3$ was 85.84 wt% Fe, with no Al, Si, or Ca.

The XRD spectrum of both samples presented the three major peaks of Fe^0, with the major reflection occurring at $\approx 44.7°$, which is characteristic of zero-valent iron while the peak at $\approx 34.8°$ indicated the presence of the iron oxide (FeO) crystalline phase (Sun et al. 2006). FeO is not a stable valence state and usually oxidises to Fe^{3+}, to form the stable magnetite mineral phase (Fe_3O_4). Since the two forms of nano Fe exhibited the same crystalline pattern, this implies that the hematite and maghemite mineral concentrate, which were the primary iron constituents of the raw CFA, served as an adequate 'ferric salt', and produced a Fe^{3+} solution after acid digestion. Reductive
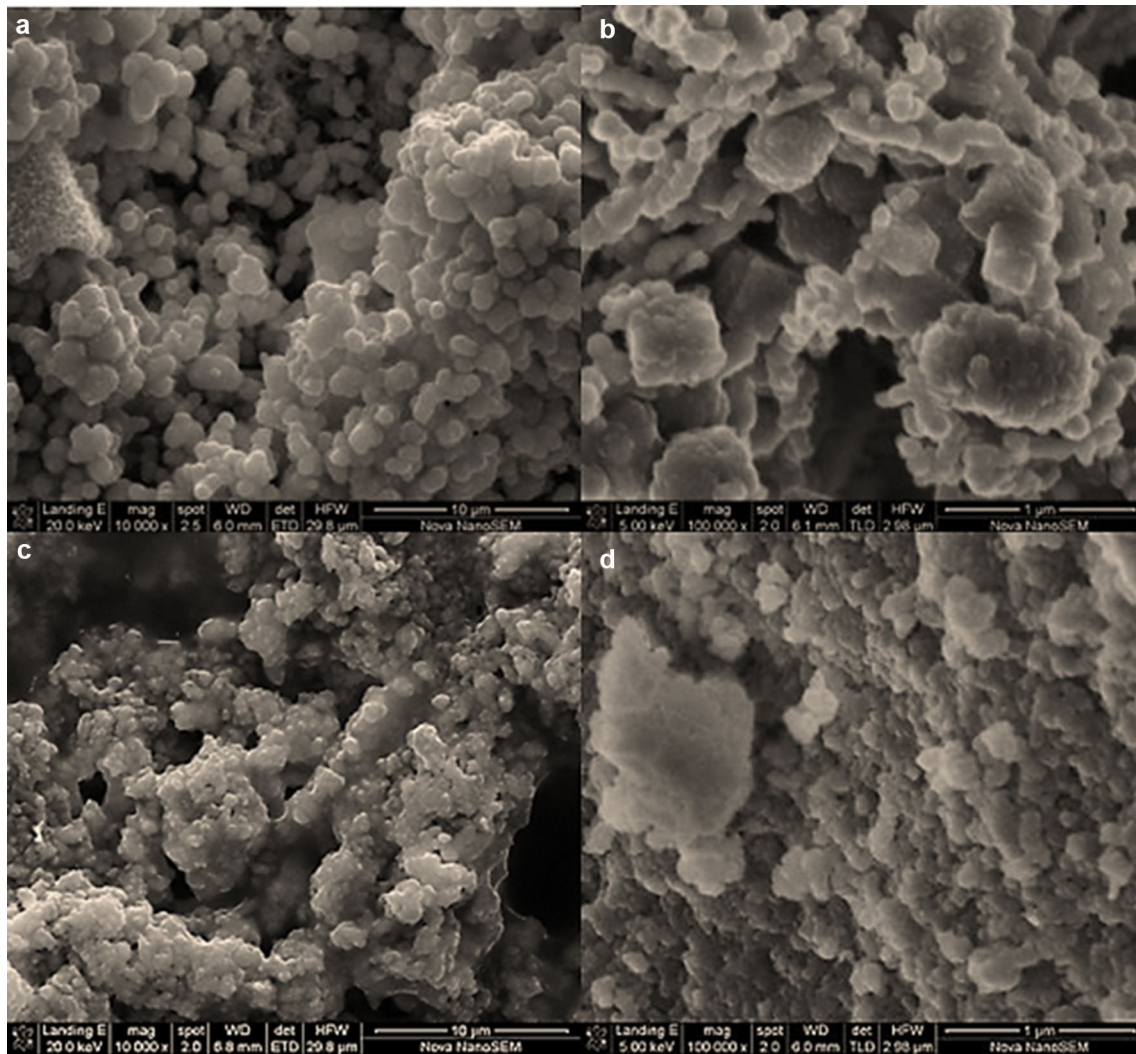
Table 5 BET parameters of the iron extracted from Hendrina coal fly ash

BET parameter	Hendrina CFA iron
BET (m^2/g)	1.34 ± 0.05
Micropore area (m^2/g)	0.02 ± 0.01
Micropore volume (m^3/g)	0.00001 ± 0.00
External surface area	1.32 ± 0.03

Fig. 4 Yield of nano Fe obtained with 100 mL of various concentrations of $NaBH_4$ used to precipitate nano Fe from 50 mL of 0.16 M granular iron digestate and 0.1 M $FeCl_3$ solution

Fig. 5 SEM micrograph of nano Fe from: granular Fe digestate at ×10,000 magnification (**a**); granular Fe digestate at ×100,000 magnification (**b**); FeCl$_3$ at ×10,000 magnification (**c**); FeCl$_3$ at ×100,000 magnification (**d**)

precipitation converted the hematite and maghemite to magnetite. The weakly diffracted, broad peaks is attributed to the particle size, signifying that this material is primarily nanosized. The particle size of the nano Fe generated from the magnetically extracted granular Fe digestate or FeCl$_3$ was determined using the XRD data in Fig. 9 and Scherrer's equation (Eq. 3):

$$\tau = \frac{K\lambda}{\beta \cos \theta} \tag{3}$$

where τ is the mean size of the ordered (crystalline) domains, which may be smaller or equal to the grain size, K is a dimensionless shape factor, with a value close to unity, λ is the X-ray wavelength, β is the line broadening at half the maximum intensity, after subtracting the instrumental line broadening, in radians, and θ is the Bragg angle.

The calculated particle size of the nano Fe extracted from the granular Fe digestate was 48.98 nm, while the nano Fe from FeCl$_3$ had a particle size of 46.36 nm. This was slightly smaller than the nano Fe from the granular Fe digestate. These values are relatively close to each other and corroborate a particle size of 40–50 nm for both nano Fe sources, as indicated by the HRTEM. The BET surface areas of the nano Fe extracted from CFA or FeCl$_3$ were 34.7 or 88.8 m^2/g, respectively. Thus, the BET surface area of nano Fe from FeCl$_3$ was more than twice that of the nano Fe extracted from CFA. A possible reason for the lower surface area could be elements such as Al, Si, and Ca that were present in the granular Fe digestate precursor. The inclusion of these components could have altered the surface chemistry of the nano Fe extracted from the CFA, and possibly caused pore blockage, thus diminishing the surface adsorption of N$_2$, resulting in less surface area.
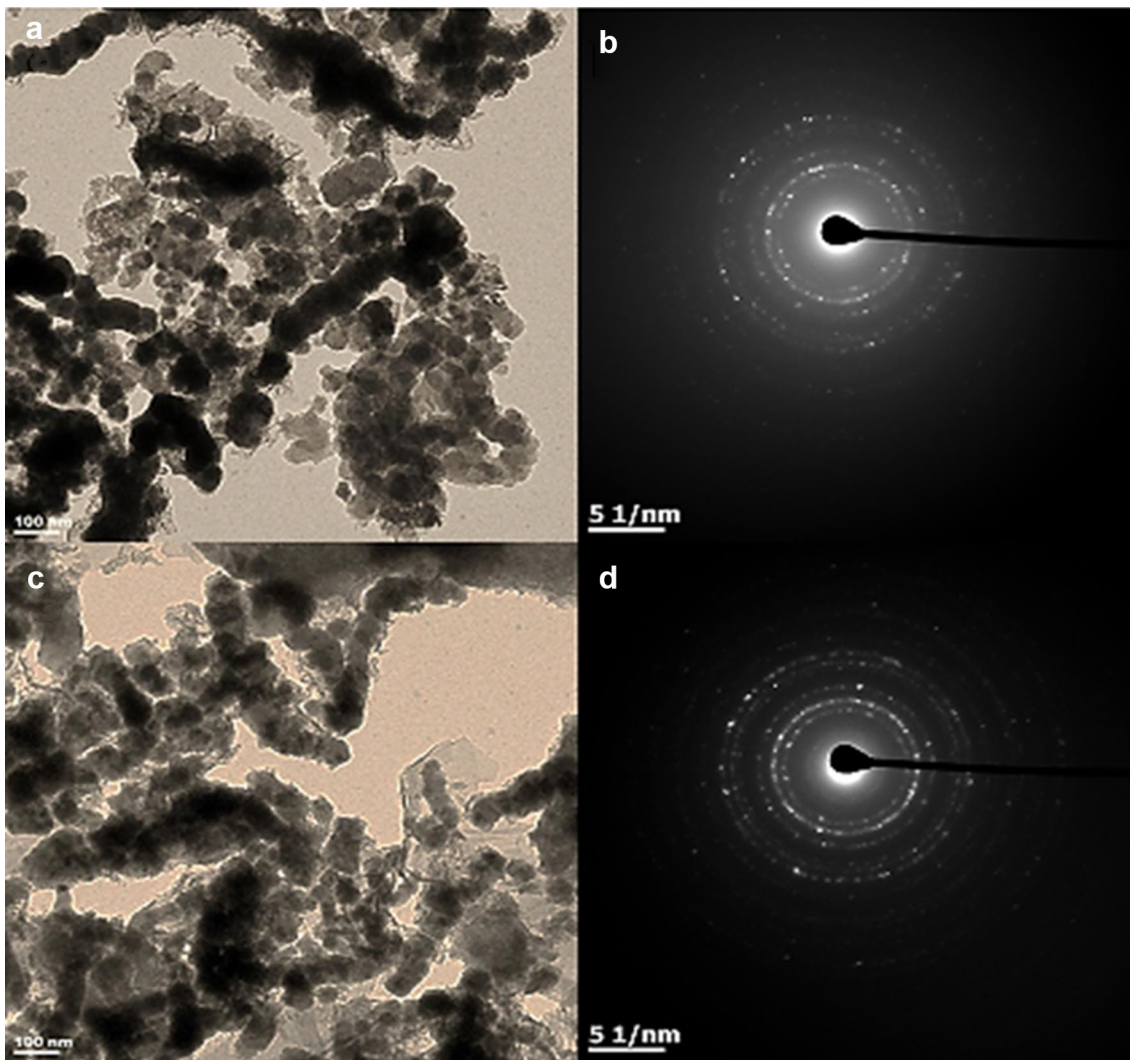
Fig. 6 HRTEM micrographs of nano Fe from: granular Fe digestate (**a**), FeCl$_3$ (**b**) and their respective SAED

Treatment of Acid Mine Drainage

For comparative purposes, the nano Fe produced were compared in the adsorption experiment to determine whether the nano Fe from CFA could compete with the reagent based nanoparticles in terms of adsorption capacity. The effects of nano Fe dosage and contact time were investigated.

The physical characteristics of the AMD were monitored during the dosage optimisation experiment for 24 h to determine changes in pH, EC, and TDS (Fig. 10a). The pH rose with the 0.1 g nano Fe per 50 mL AMD dosage, after which there was a decrease. The increase in pH can be attributed for all samples to the hydrolysis of water by the nano iron, which releases OH$^-$ ions into the solution (Eq. 4).

$$Fe^0 + 2H_2O \rightarrow Fe^{2+} + H_2 + 2OH^- \tag{4}$$
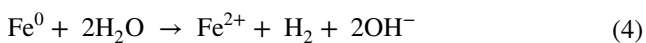
After the 24 h contact time, the 0.1 g sample had the highest pH value (4.98), with an EC value of 3.01. Aliquots of AMD for each dose were submitted for elemental analysis by ICP-OES after 24 h to determine the concentration of elements present in the AMD after treatment.

The ICP-OES result (supplemental Figure S-5) shows the concentration of the cations in the AMD after treatment with 0.1 g dosage of nano Fe generated from the granular iron digestate or FeCl$_3$. Figure S-5 indicates that the level of cations in the AMD were drastically reduced after the treatment processes using both forms of nano Fe. Although, the removal capacities of the two materials follow a similar trend, Li, Sr, Ba, B, Al, Na, and Co were all removed from the AMD to some extent by the nano Fe extracted from FeCl$_3$, but not at all by nano Fe extracted from CFA. Conversely, K, Mn, and Ti were removed by the nano Fe
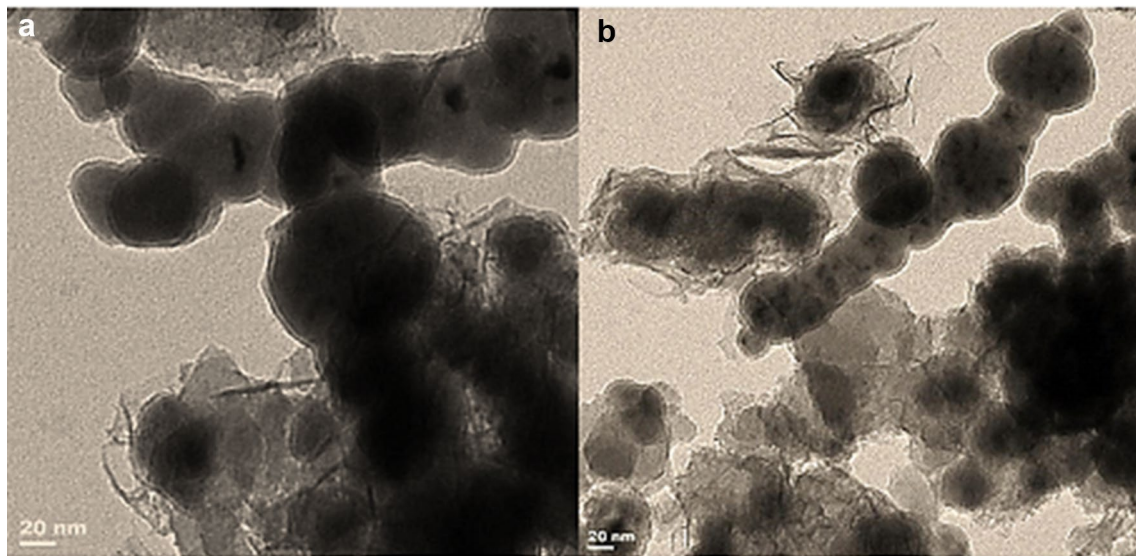
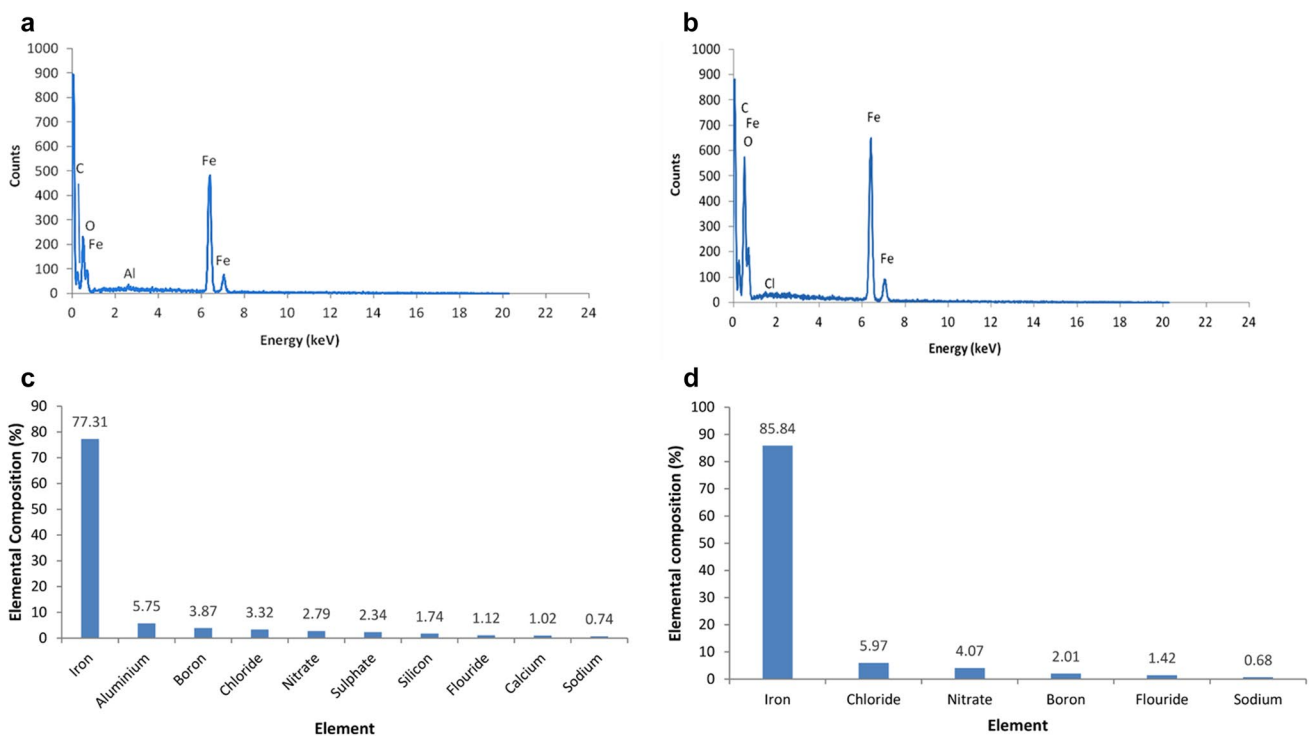**Fig. 7** HRTEM micrographs of iron nano Fe precipitated from: granular Fe digestate (**a**), or $FeCl_3$ (**b**)

Fig. 8 EDS analysis of nano Fe from granular Fe digestate (**a**) or $FeCl_3$ (**b**); quantitative elemental analysis of nano Fe from granular Fe digestate (**c**), or $FeCl_3$ (**d**)

extracted from CFA but not by the nano Fe extracted from $FeCl_3$. This might be due to difference in the purity of the extracted nano Fe (Fig. 8c, d).

Effect of Contact Time

The contact time was optimised to determine whether a shorter agitation time would suffice and to determine if the time frame was related to the leaching experienced with the

Fig. 9 X-ray diffractogram of nano Fe from granular digestate (FANI) or FeCl$_3$ (FCLI)
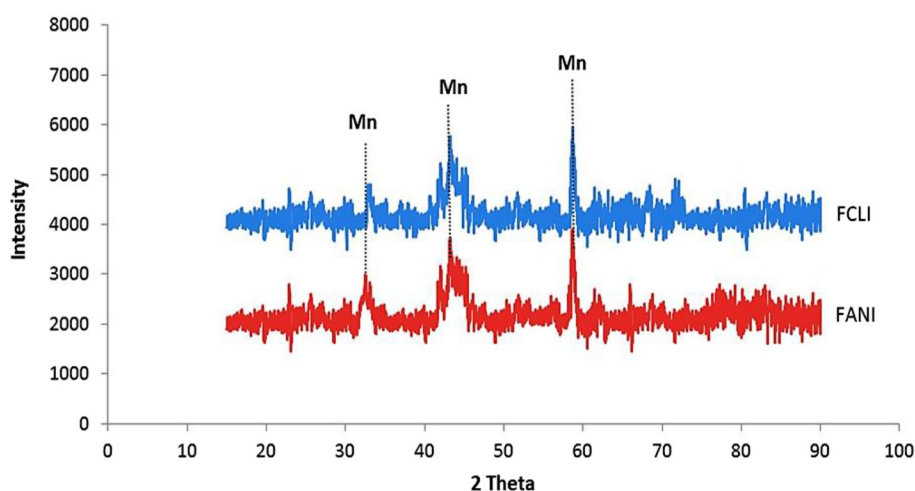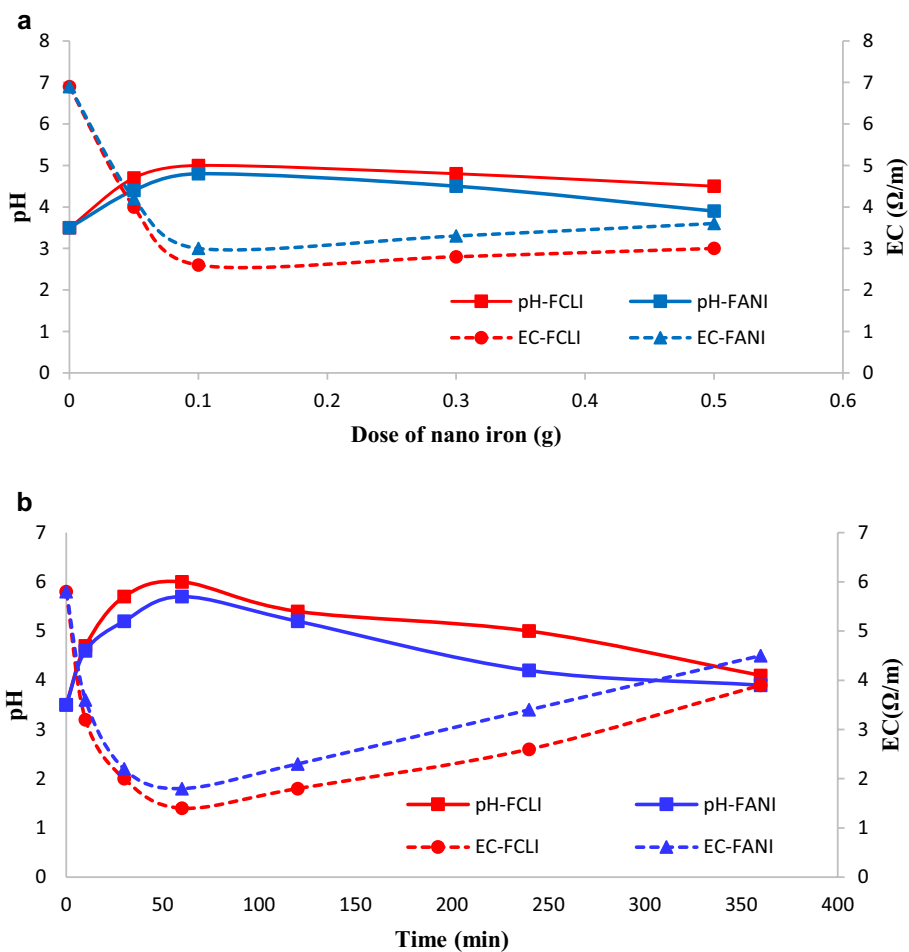

Fig. 10 **a** Effect of nano Fe dosage (obtained from granular Fe digestate (FANI) or FeCl$_3$ (FCLI)) on the pH and EC of AMD, using a contact time of 24 h, **b** effect of contact time on the pH and EC of the treated AMD using 0.1 g of nano Fe extracted from the granular Fe digestate (FANI) or FeCl$_3$ (FCLI)

24 h period. Figure 10b illustrates the changes in pH and EC that occurred in the batch experiment using the optimised dosage of 0.1 g of nano Fe from either source, while contact time was varied.

The pH of the treated AMD under the optimised conditions (1 h) using the nano Fe from CFA was increased from 3.49 to 5.74, whereas the pH of the AMD after treatment with nano Fe from FeCl$_3$ was increased to 6.01. Many of

Table 6 Elemental analysis of the treated AMD after the addition of 0.1 g of nano Fe extracted from CFA or $FeCl_3$, at contact time of 1 h

Element (mg/L)	AMD treated with nano Fe from CFA	AMD treated with nano Fe from $FeCl_3$	Category 4 industrial use guideline
SO_4^{2-}	1469 ± 1	1759 ± 2	500.00
Ca	281 ± 1	574 ± 1	300.00
Na	282 ± 4	239 ± 7	NR
Mg	155 ± 6	208 ± 7	NR
K	55 ± 3	17 ± 3	NR
Fe	185 ± 5	158 ± 11	100
Mn	50 ± 4	67 ± 6	100.00
Cl^-	40 ± 1	167 ± 5	NR
Si	82 ± 3	84 ± 3	150
NO_3^-	12 ± 1	11 ± 1	NR
B	16 ± 1	37 ± 4	NR
Hg	3.8 ± 0.3	3 ± 1	NR
Li	0.05 ± 0.01	0.10 ± 0.02	NR
Al	4 ± 1	3.3 ± 0.1	NR
Se	0.7 ± 0.4	2.2 ± 0.1	NR
U	0.14 ± 0.01	0.5 ± 0.2	NR
Th	0.6 ± 0.2	0.09 ± 0.03	NR
Ni	0.4 ± 0.1	1.2 ± 0.1	NR
Zn	0.12 ± 0.02	0.3 ± 0.1	NR
Co	0.41 ± 0.04	0.7 ± 0.2	NR
Ce	0.04 ± 0.01	0.06 ± 0.01	NR
P	0.7 ± 0.2	0.34 ± 0.09	NR
Sr	0.5 ± 0.1	0.6 ± 0.1	NR
Pb	0.24 ± 0.08	0.21 ± 0.04	NR
Ba	0.5 ± 0.1	0.09 ± 0.02	NR
As	0.5 ± 0.1	0.5 ± 0.1	NR
Cr	0.4 ± 0.1	0.5 ± 0.2	NR
Cu	0.13 ± 0.03	0.07 ± 0.02	NR
Mo	0.04 ± 0.01	0.05 ± 0.02	NR
Rb	0.01 ± 0.00	0.02 ± 0.01	NR
Ti	0.11 ± 0.02	0.12 ± 0.03	NR
Nb	0.03 ± 0.01	0.12 ± 0.01	NR
Zr	0.07 ± 0.03	0.11 ± 0.02	NR
Y	0.02 ± 0.01	0.05 ± 0.01	NR
V	0.01 ± 0.00	0.05 ± 0.02	NR
Cd	0.01 ± 0.00	0.02 ± 0.01	NR
Be	0.01 ± 0.00	0.01 ± 0.00	NR
F^-	67 ± 5	58 ± 6	NR

NR not reported

the contaminants were reduced and adsorbed onto the Fe or precipitated, thus decreasing the TDS concentration and hence the EC of the AMD.

A comparison of these processes for the nano Fe from both sources revealed that desorption may have occurred at different rates and to a different extent for each sample. The gradual decrease in pH and increase in EC of the nano Fe obtained from $FeCl_3$ may imply that it was able to retain the adsorbed species for a longer period of time, as opposed to the nano Fe from the granular Fe digestate, which displayed a faster decrease in pH and increase in EC. The final values of the nano Fe extracted from the granular iron digestate also resulted in a slightly lower pH and higher EC than that of the nano Fe from $FeCl_3$. This may have been affected by the fact that the nano Fe extracted from the granular Fe digestate removed less of the major AMD contaminants.

The data (Table 6) indicates that with the exception of sulphate, most of the other constituents of the AMD treated

with the nano Fe made from the granular Fe digestate or $FeCl_3$ are below the DWAF effluent limits required for Category 4 industrial use. Also, although the sulphate exceeded the effluent limit, about 70% and 65% of the sulphate was removed by the nano Fe obtained from CFA or $FeCl_3$, respectively.

The concentrations of all elements decreased after 1 h. Moreover, the CFA and $FeCl_3$ nano Fe exhibited similar removal capabilities and generally followed the same trend, working equally well in treating the AMD.

Conclusion

The current way CFA is disposed of poses an environmental concern due to the possibility that contaminants can leach into the environment. Likewise, the discharge of untreated AMD can cause severe environmental problems to soil, surface, and ground water. The focus of this research were to ascertain if a waste such as CFA could be used for the preparation of nano Fe and to determine if the nano Fe from CFA was comparable to nano Fe generated from reagent grade chemicals for AMD treatment. The experimental results confirmed that the nano Fe produced by the two techniques have similar properties and exhibited the same crystalline pattern. The AMD remediation capability of the nano Fe from the two sources shows that the optimum nano Fe dosage and contact time were 0.002 g/ml (0.1 g nano Fe/50 mL AMD) and 1 h, respectively. Under these conditions, Pb, P, Se, Rb, Ni, Li, K, Mo, Mn, V, Y, Th, Zn, Zr, Hg, Sr, Ti, Nb, Be, As, Al, Ca, Ba, B, U, Mg, Cu, Cr, Fe, Na, Cd, Co, Ce, Cl^-, and SO_4^{2-} were decreased in the treated AMD. The nano Fe extracted from CFA had a similar removal capability to that obtained from $FeCl_3$, with the exception of a few elements such as Pb, Ba, Al, and Na. In terms of the metal content, the resulting water was deemed to be suitable for Category 4 industrial use, per the DWAF allowed limits. It should be noted that the composition of nano Fe will vary when other sources are considered and that the presence and types of impurities will also affect the quality of the nano Fe. Finally, future investigation comparing the costs of AMD treatment by nano Fe extracted from CFA or $FeCl_3$ is required to validate the feasibility and applicability of nano Fe to AMD treatment.

References

Ali A, Hira Zafar MZ, ul Haq I I, Phull AR, Ali JS, Hussain A (2016) Synthesis, characterization, applications, and challenges of iron oxide nanoparticles. Nanotechnol Sci Appl 9:49

Brooke R, Cottis P, Talemi P, Fabretto M, Murphy P, Evans D (2017) Recent advances in the synthesis of conducting polymers from the vapour phase. Prog Mater Sci 86:127–146

Cao J, Elliott D, Zhang W (2005) Perchlorate reduction by nanoscale iron particles. J Nanopart Res 7:499–506

Cao M, Li Z, Wang J, Ge W, Yue T, Li R, Colvin VL, Yu WW (2012) Food related applications of magnetic iron oxide nanoparticles: enzyme immobilization, protein purification, and food analysis. Trends Food Sci Technol 27(1):47–56

Carpenter EE (2001) Iron nanoparticles as potential magnetic carriers. J Magn Magn Mater 225:17–20

Choi SK, Lee S, Song YK, Moon HS (2002) Leaching characteristics of selected Korean fly ashes and its implications for the groundwater composition near the ash disposal mound. Fuel 81(8):1083–1090

Dai BQ, Wu X, De Girolamo A, Cashion J, Zhang L (2015) Inhibition of lignite ash slagging and fouling upon the use of a silica-based additive in an industrial pulverised coal-fired boiler: part 2. Speciation of iron in ash deposits and separation of magnetite and ferrite. Fuel 139:733–745

Dolores R, Raquel S, Adianez GL (2015) Sonochemical synthesis of iron oxide nanoparticles loaded with folate and cisplatin: effect of ultrasonic frequency. Ultrason Sonochem 23:391–398

DWAF (Dept. of Water Affairs and Forestry) (2005) Minimum requirements for the handling, classification and disposal of hazardous waste: section 10 waste handling, storage and transportation, 3rd edn. Pretoria, pp 94–111

Eberhard A (2011) The future of South African coal: market, investment, and policy challenges. http://iis-db.stanford.edu/pubs/23082/WP_100_Eberhard_Future_of_South_African_Coal.pdf. Accessed 4 Nov 2013

Elliott D, Cao J, Zhang W, Spear S (2003) Nanoscale iron particles for perchlorate reduction. In: The 225th ACS National meeting, 43. New Orleans, LA, United States, p 564

Farhanian D, Dorval Dion CA, Raphael W, De Crescenzo G, Tavares JR (2014) Combined extraction and functionalization of low-cost nanoparticles from municipal solid waste fly ash through PICVD. J Environ Chem Eng 2:2242–2251

Fashola MO, Ngole-Jeme VM, Babalola OO (2016) Heavy metal pollution from gold mines: environmental effects and bacterial strategies for resistance. Int J Environ Res Public Health 13(11):1047. https://www.ncbi.nlm.nih.gov/pmc/articles/PMC5129257

Font O, Querol X, Juan R, Casado R, Ruiz CR, López-Soler Á, Coca P, Peña FG (2007) Recovery of gallium and vanadium from gasification fly ash. J Hazard Mater 139(3):413–423

Geng B, Jin Z, Li T, Qi X (2009) Preparation of chitosan-stabilized Fe^0 nanoparticles for removal of hexavalent chromium in water. Sci Total Environ 407(18):4994–5000

Gitari MW, Petrik LF, Etchebers O, Key DL, Iwuoha E, Okujeni C (2006) Treatment of acid mine drainage with fly ash: removal of major contaminants and trace elements. J Environ Sci Health A 41:1729–1747

Gray NF (1998) Acid mine drainage composition and the implications for its impact on lotic systems. Water Res 32(7):2122–2134

Groen JC, Craig JR (1994) The inorganic geochemistry of coal, petroleum, and their gasification/combustion products. Fuel Process Technol 40(1):15–48

Gui L, Gillham RW, Odziemkowski MS (2000) Reduction of N-nitrosodimethylamine with granular iron and nickel-enhanced iron. 1. Pathways and kinetics. Environ Sci Technol 34(16):3489–3494

Huang KC, Ehrman SH (2007) Synthesis of iron nanoparticles via chemical reduction with palladium ion seeds. Langmuir 23(3):1419–1426

Huber DL (2005) Synthesis, properties, and applications of iron nanoparticles. Small 1(5):482–501

Hufschmid R, Arami H, Ferguson RM, Gonzales M, Teeman E, Brush LN, Browning ND, Krishnan KM (2015) Synthesis of phase-pure

and monodisperse iron oxide nanoparticles by thermal decomposition. Nanoscale 7(25):11142–11154

Jeen SW, Gillham RW, Blowes DW (2006) Effects of carbonate precipitates on long-term performance of granular iron for reductive dechlorination of TCE. Environ Sci Technol 40(20):6432–6437

Kapoor S, Christian RA (2016) Transport of toxic elements through leaching in and around ash disposal sites. Int J Environ Sci Dev 7(1):65–68

Kerekes L, Hakl J, Mészáros S, Vad K, Gurin P, Kis-Varga M, Uzonyi I, Szabó S, Beke DL (2002) Study of magnetic relaxation in partially oxidized nanocrystalline iron. Czech J Phys 52(1):A89–A92

Kim H, Hong HJ, Jung J, Kim SH, Yang JW (2010) Degradation of trichloroethylene (TCE) by nanoscale zero-valent iron (nZVI) immobilized in alginate bead. J Hazard Mater 176(1–3):1038–1043

Kutchko BG, Kim AG (2006) Fly ash characterization by SEM–EDS. Fuel 85(17–18):2537–2544

Li XQ, Zhang WX (2007) Sequestration of metal cations with zerovalent iron nanoparticles. A study with high resolution X-ray photoelectron spectroscopy (HR-XPS). J Phys Chem C 111(19):6939–6946

Li XQ, Elliott DW, Zhang WX (2006) Zero-valent iron nanoparticles for abatement of environmental pollutants: materials and engineering aspects. Crit Rev Solid State Mater Sci 31:111–122

Liu Y, Majetich SA, Tilton RD, Sholl DS, Lowry GV (2005) TCE dechlorination rates, pathways, and efficiency of nanoscale iron particles with different properties. Environ Sci Technol 39:1338–1345

Martin JE, Herzing AA, Yan W, Li XQ, Koel BE, Kiely CJ, Zhang WX (2008) Determination of the oxide layer thickness in core–shell zerovalent iron nanoparticles. Langmuir 24(8):4329–4334

Mattigod SV, Rai D, Eary LE, Ainsworth CC (1990) Geochemical factors controlling the mobilization of inorganic constituents from fossil fuel combustion residues: review of the major elements. J Environ Qual 19:188–201

Mueller NC, Nowack B (2010) Nano zero valent iron—the solution for water and soil remediation? Report of the ObservatoryNANO. Available online at www.observatorynano.eu. Accessed 22 Mar 2011

Nurmi JT, Tratnyek PG, Sarathy V, Baer DR, Amonette JE, Pecher K, Wang C, Linehan JC, Matson DW, Penn RL, Driessen MD (2005) Characterization and properties of metallic iron nanoparticles: spectroscopy, electrochemistry, and kinetics. Environ Sci Technol 39(5):1221–1230

Nutt M, Hughes JB, Wong M (2005) Designing Pd-on-Au bimetallic nanoparticle catalysts for trichloroethylene hydrodechlorination. Environ Sci Technol 39(5):1346–1353

Polowczyk I, Ulatowska J, Koźlecki T, Bastrzyk A, Sawiński W (2013) Studies on removal of boron from aqueous solution by fly ash agglomerates. Desalination 310(1):93–101

Ponder SM, Darab JG, Mallouk TE (2000) Remediation of Cr(VI) and Pb(II) aqueous solutions using supported, nanoscale zerovalent iron. Environ Sci Technol 34(12):2564–2569

Pradoto R, Moini MR, Flores-Vivian I, Kozhukova M, Sobolev K (2016) Fly ash-nano SiO_2 blends for effective application in self-consolidating concrete. In: Khayat KH (ed) Proceedings of 8th international RILEM Symposium on self-compacting concrete. Washington DC, pp 299–308

Sahoo PK, Kim K, Powell MA, Equeenuddin SM (2016) Recovery of metals and other beneficial products from coal fly ash: a sustainable approach for fly ash management'. Int J Coal Sci Technol (China) 3(3):267–283

Scherer MM, Johnson KM, Westall JC, Tratnyek PG (2001) Mass transport effects on the kinetics of nitrobenzene reduction by iron metal. Environ Sci Technol 35(13):2804–2811

Shahwan T, Üzüm Ç, Eroğlu AE, Lieberwirth I (2010) Synthesis and characterization of bentonite/iron nanoparticles and their application as adsorbent of cobalt ions. Appl Clay Sci 479(3–4):257–262

Shih Y, Tai Y (2010) Reaction of decabrominated diphenyl ether by zerovalent iron nanoparticles. Chemosphere 78(10):1200–1206

Shoumkova AS (2011) Magnetic separation of coal fly ash from Bulgarian power plants. Waste Manag Res 29:1078–1089

Silva LFO, Moreno T, Querol X (2009) An introductory TEM study of Fe-nanominerals within coal fly ash. Sci Total Environ 407:4972–4974

Sun Y, Takaoka M, Takeda N, Matsumoto T, Oshita K (2006) Kinetics on the decomposition of polychlorinated biphenyls with activated carbon-supported iron. Chemosphere 65:183–189

Torralvo FA, Fernández-Pereira C (2011) Recovery of germanium from real fly ash leachates by ion-exchange extraction. Miner Eng 24(1):35–41

Üzüm Ç, Shahwan T, Eroğlu AE, Hallam KR, Scott TB, Lieberwirth I (2009) Synthesis and characterization of kaolinite-supported zero-valent iron nanoparticles and their application for the removal of aqueous Cu^{2+} and Co^{2+} ions. Appl Clay Sci 43(2):172–181

Varanasi P, Fullana A, Sidhu S (2007) Remediation of PCB contaminated soils using iron nano-particles. Chemosphere 66(6):1031–1038

Wang S, Ma Q, Zhu ZH (2008) Characteristics of coal fly ash and adsorption application. Fuel 87(15–16):3469–3473

Wang Q, Snyder S, Kim J, Choi H (2009) Aqueous ethanol modified nanoscale zerovalent iron in bromate reduction: synthesis, characterization, and reactivity. Environ Sci Technol 43(9):3292–3299

WHO (World Health Organization) (2011) Guidelines for drinking-water quality, 4th edition. Geneva. http://www.who.int/iris/handle/10665/44584. Accessed 18 July 2018

Wu GH, Dou ZY, Jiang LT, Cao JH (2006) Damping properties of aluminium matrix-fly ash composites. Mater Lett 60(24):2945–2948

Xiao Z, Mitchell BS (2000) Mullite decomposition kinetics and melt stabilization in the temperature range 1900–2000 °C. J Am Ceram Soc 83(4):761–767

Zhang W (2003) Nanoscale iron particles for environmental remediation: an overview. J Nanopart Res 5(3–4):323–332